Earth Pressure due to Vibratory Compaction

Tsang-Jiang Chen[1] and Yung-Show Fang, M.ASCE[2]

Abstract: This paper presents experimental data on the variation of lateral earth pressure against a nonyielding retaining wall due to soil filling and vibratory compaction. Air-dry Ottawa sand was placed in five lifts and each lift was compacted to achieve a relative density of 75%. Each compacted lift was 0.3 m thick. The instrumented nonyielding wall facility at National Chiao Tung University in Taiwan was used to investigate the effects of vibratory compaction on the change of stresses at the soil-wall interface. Based on the experimental data it has been found that, for a compacted backfill, the vertical overburden pressure can also be properly estimated with the traditional equation $\sigma_v = \gamma z$. The effects of vibratory compaction on the vertical pressure in the backfill were insignificant. On the vertical nonyielding wall, extra horizontal earth pressure was induced by vibratory compaction. After compaction, the lateral earth pressure measured near the top of the wall was almost identical to the passive Rankine pressure. It is concluded that as the cyclic compacting stress applied on the surface of the backfill exceeded the ultimate bearing capacity of the foundation soil, a shear failure zone would develop in the uppermost layer of the backfill. For a soil element under lateral compression, the vertical overburden pressure remained unchanged, and the horizontal stress increased to the Rankine passive pressure. It was also found that the compaction-influenced zone rose with the rising compaction surface. The horizontal earth pressure measured below the compaction-influenced zone converged to the Jaky state of stress.

DOI: 10.1061/(ASCE)1090-0241(2008)134:4(437)

CE Database subject headings: Soil compaction; Earth pressure; Model tests; Retaining walls; Sand.

Introduction

Compaction is a particular kind of soil stabilization and one of the oldest methods for improving existing soil or man-placed fills. The objective of the compaction operation is to improve the engineering properties of soil such as increasing the fill's bearing capacity or reducing settlement. For granular soils, achieving a relative density of 70–75% is generally recommended (US Navy 1982). Hand tampers and vibratory compaction equipment are commonly used to compact the fill.

Conventionally, the earth pressure at rest is evaluated by the Jaky equation (Jaky 1944). Based on their laboratory tests, Sherif et al. (1984) found that the Jaky's equation ($K_o = 1 - \sin\phi$) gives good results when the backfill is loose sand, where K_o=coefficient of earth pressure at rest and ϕ=internal friction angle of soil. When the backfill behind the wall is either compacted or vibrated to increase its density, the magnitude of at-rest stresses increases due to densification.

Based on the concept of hysteretic loading and unloading behavior, Duncan and Seed (1986) developed a procedure to estimate the magnitude of the peak and residual compaction-induced earth pressure both in the free field and acting against a vertical nonyielding wall. Peck and Mesri (1987) presented a method to evaluate the compaction-induced earth pressure. Near the surface of backfill, the lateral pressure on the wall is subject to the passive failure condition. In the lower part of the backfill, the lateral pressure is directly related to the effective overburden pressure. Duncan et al. (1991) used the analytical procedures proposed by Duncan and Seed (1986) to develop earth pressure charts and tables that can be used to estimate residual earth pressure due to compaction quickly.

Unfortunately, in the previous studies, little information has been reported regarding the variation of stress condition in the soil mass during the filling and compaction process. This paper presents experimental data associated with the lateral earth pressure acting on a nonyielding wall at different stages of soil filling and compaction. Based on the experimental data, a possible mechanism of soil behavior under vibratory loading is proposed. All of the experiments mentioned in this paper were conducted in the National Chiao Tung University (NCTU) nonyielding retaining wall facility, which is briefly described in the following section. Horizontal earth pressure against the wall was measured with the soil-pressure transducer (SPT) mounted on the wall, and the vertical earth pressure was measured with transducers buried in the backfill. It is hoped that these test results might enhance a better understanding regarding the development of compaction-induced earth pressure during construction.

NCTU Nonyielding Retaining-Wall Facility

The entire facility consists of three components, namely, model retaining wall, soil bin, and data acquisition system.

Model Retaining Wall

The model wall shown in Fig. 1 is 1.5 m wide and 1.6 m high. The wall is 45 mm thick and made of a solid steel plate. To

[1]Geotechnical Engineer, Mass Transportation Engineering Dept. II, Sinotech Engineering Consultants, Ltd., Taipei 105, Taiwan; formerly, Ph.D. Candidate, Dept. of Civil Engineering, National Chiao Tung Univ., Hsinchu 30010, Taiwan.

[2]Professor and Dean, College of Engineering, National Chiao Tung Univ., Hsinchu, 30010, Taiwan, R.O.C. (corresponding author). E-mail: ysfang@mail.nctu.edu.tw

Note. Discussion open until September 1, 2008. Separate discussions must be submitted for individual papers. To extend the closing date by one month, a written request must be filed with the ASCE Managing Editor. The manuscript for this paper was submitted for review and possible publication on February 24, 2006; approved on August 11, 2007. This paper is part of the ***Journal of Geotechnical and Geoenvironmental Engineering***, Vol. 134, No. 4, April 1, 2008. ©ASCE, ISSN 1090-0241/2008/4-437–444/$25.00.

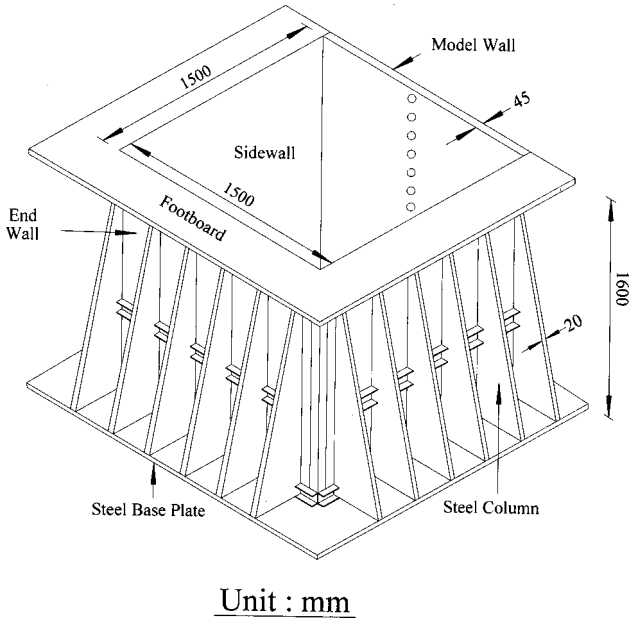

Fig. 1. NCTU nonyielding retaining-wall facility

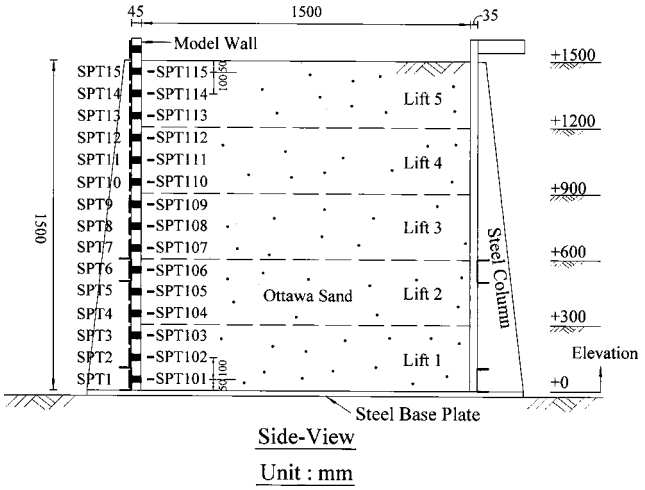

Fig. 2. Locations of soil pressure transducers

achieve an at-rest condition, the major factor considered in choosing the wall material is rigidity. It is clear in Fig. 1 that the model wall is actually the front side of the reinforced steel box. Outside the box, 24 20-mm-thick steel columns were welded on the walls to reduce any lateral displacement during loading. In addition, 12 channel section steel beams were welded horizontally around the box to further increase the stiffness of the soil bin.

Soil Bin

The soil bin was fabricated of steel plates with inside dimensions of 1.5 m × 1.5 m × 1.6 m as illustrated in Fig. 1. The end wall and sidewalls of the soil bin were made of 35-mm thick steel plates. To constitute a plane-strain condition, the soil bin was built very rigid so that the lateral deformation of sidewalls under soil pressure would be negligible.

The model wall, sidewalls, end wall, and base plate of the soil bin were welded together to reduce flexibility. The bottom of the soil bin was covered with a layer of SAFETY WALK, which is an antislip frictional material to provide adequate friction between the soil and the base of the bin.

To investigate the distribution of earth pressure with depth, soil pressure transducers were attached to the model wall as illustrated in Fig. 2. Fifteen transducers SPT1–SPT15 (Kyowa PGM-02KG, capacity=19.6 kN/m^2) were arranged within the central zone of the model wall to measure the horizontal earth pressure σ_h acting on the model wall. To investigate the development of vertical stress in the backfill, another series of soil pressure transducers (SPTs) SPT101–SPT115 (Kyowa BE-2KCM17, capacity =98.0 kN/m^2) were buried behind the model wall as illustrated in Fig. 2. These transducers were used to measure the variation of vertical earth pressure σ_v in the backfill during the filling and compaction process.

Data Acquisition System

Due to the considerable amount of data collected during the test, a data acquisition system was used. The analog signals from the sensors were filtered and amplified by the dynamic strain amplifiers (Kyowa, DPM-711B), then digitized by an analog-to-digital converter. The digital signal was then transmitted to the computer for storage and analysis. For more information regarding the NCTU nonyielding retaining-wall facility and the calibration of transducers, the readers are referred to Chen and Fang (2002) and Chen (2003).

Backfill and Interface Characteristics

Air-dry Ottawa sand was used for the model wall experiments. Physical properties of the soil included G_s=2.65; e_{max}=0.76; e_{min}=0.50; D_{60}=0.39 mm; and D_{10}=0.26 mm. To achieve the loose condition, Ottawa sand was deposited by air pluviation from the slit of a hopper into the soil bin. The drop distance was approximately 1.0 m from the soil surface throughout the placement process.

The distribution of relative density with depth in the loose sand is shown in Fig. 3. It is clear that the soil density was relatively uniform in the soil mass. The dashed lines on the left-hand side represent the mean of relative density 31% ±1 SD 2.3%.

To simulate the backfill compacted in the field, the loose backfill was placed and compacted in five lifts. Each lift was pluviated into the soil bin, carefully leveled, and then compacted with a vibratory compactor. The soil surface was divided into seven lanes parallel to the face of the model wall. The lane next to the end wall was compacted first and the lane next to the model wall was compacted last. Each lane was densified with the compactor with a pass having a duration of 70 s. Each compacted lift had a thickness of 0.3 m. The vibratory compactor was made by attaching an eccentric motor (Mikasa Sangyo, KJ75-2P) to a 0.225 m × 0.225 m × 0.002 m steel plate. The total mass of the vibratory compactor was 12.1 kg. The amplitude of downward cyclic vertical force (static+dynamic) measured with a load cell placed under the base plate of the vibratory compactor was 1.767 kN, and the measured frequency of vibration was 44 Hz. Assuming the distribution of contact pressure between the base plate and soil was uniform; the downward cyclic normal stress σ_{cyc} applied to the surface of the soil was 34.9 kN/m^2. Before compaction, the thickness of the loose soil lift was 322 mm. After compaction, the thickness of the dense soil lift was 300 mm. The settlement of the soil lift due to vibratory compaction was approximately 22 mm,

J. Geotech. Geoenviron. Eng. 2008.134:437-444.

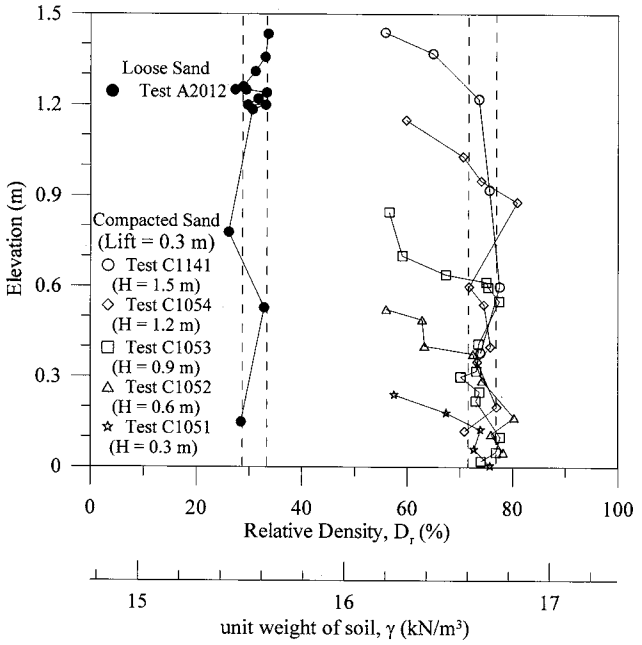

Fig. 3. Distribution of soil density with depth

which was about 6.8% of the original lift thickness. This value was in agreement with the range 3–8% of compression generally assumed for the soil layer subjected to vibratory compaction.

Fig. 3 shows the relative density profile in the compacted soil mass. The soil density was relatively uniform in the compacted fill, except for the soil near the compacted surface. The dashed lines on the right-hand side of Fig. 3 indicate the mean relative density 75% ±1 SD 2.7%. From a mean relative density of 31–75%, the effects of vibratory compaction on soil density were quite obvious. D'Appolonia et al. (1969) concluded that the low density which exists in the uppermost zone is due to vibration and lack of confinement in the sand. In this zone, the soil particles separated due to vibration and settled into a loose state when the vibration stopped.

Direct shear tests were conducted to determine the internal friction angle of the loose and compacted backfill. The 60 mm × 60 mm square shear box was placed in the soil bin, pluviated with Ottawa sand, subjected to compaction effort, extracted from the soil mass, and tested in the laboratory. Soil parameters determined for compacted and loose fills are indicated in Figs. 4(a and b).

To simulate a plane-strain condition, the shear stress between the backfill and sidewall should be minimized to be nearly frictionless. This was accomplished by creating a lubrication layer between the sidewalls and the soil. The lubrication layer consisted of two 0.009-mm thin plastic sheets and a 0.152-mm thick plastic sheet. It was expected that the thick sheet would help to smooth out the rough interface as a result of plastic sheet penetration under normal stress. Two thin sheets were placed next to the steel sidewall to provide more possible sliding planes. For more information regarding the reduction of boundary friction with the plastic-sheet method, the reader is referred to Fang et al. (2004).

Test Results

This section reports on the experimental results regarding the vertical and horizontal earth pressure in loose and compacted sand.

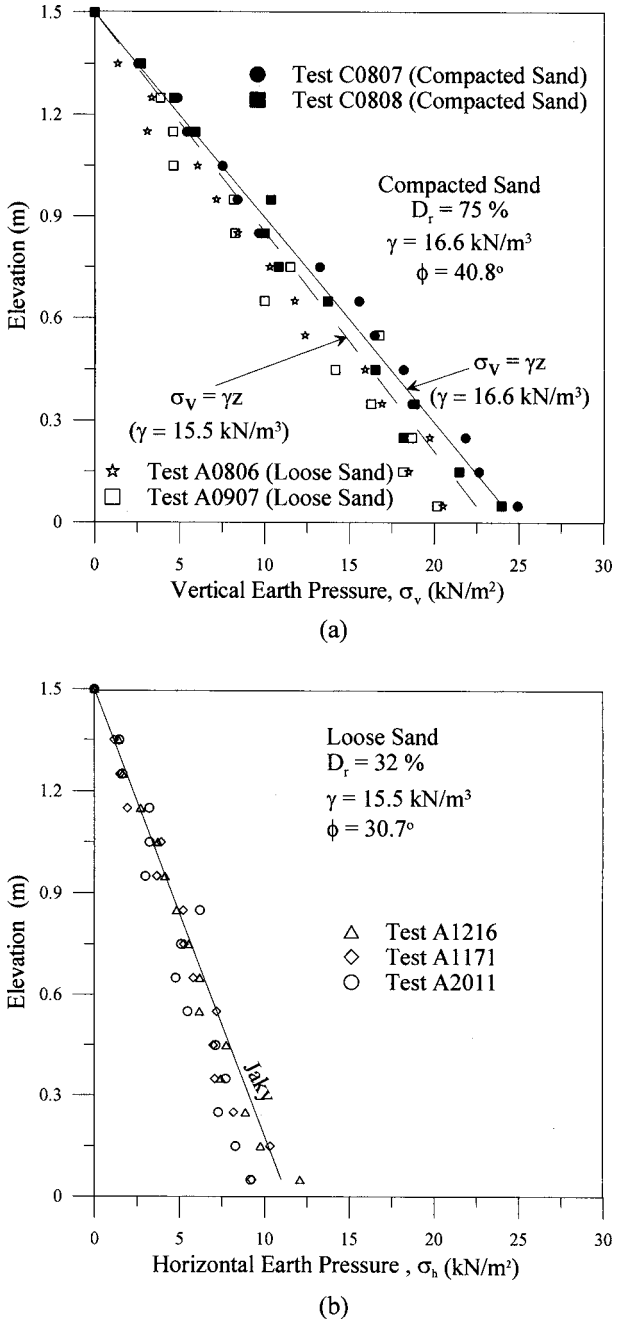

Fig. 4. (a) Distribution of vertical earth pressure measured in soil mass; (b) distribution of horizontal earth pressure against model wall

Stresses in Loose Sand

For comparison purposes, at the beginning of this study, experiments were conducted to investigate the normal stresses in the uncompacted backfill. Fig. 2 shows the location of SPT 101–115 buried in the soil mass. The distribution of vertical earth pressure σ_v measured in the soil mass is illustrated in Fig. 4(a). It can be seen that the vertical pressure increases linearly with increasing depth z and the test data are in fairly good agreement with the predicted distribution using the traditional equation $\sigma_v = \gamma z$, where γ = unit weight of backfill. The distribution of horizontal earth pressure against the nonyielding model wall is shown in Fig. 4(b). It can be seen from the figure that the at-rest pressure profile induced by the 1.5-m-thick loose fill is approximately linear. Jaky's equation $\sigma_h = \sigma_v(1 - \sin\phi)$ slightly overestimates the hori-

J. Geotech. Geoenviron. Eng. 2008.134:437-444.

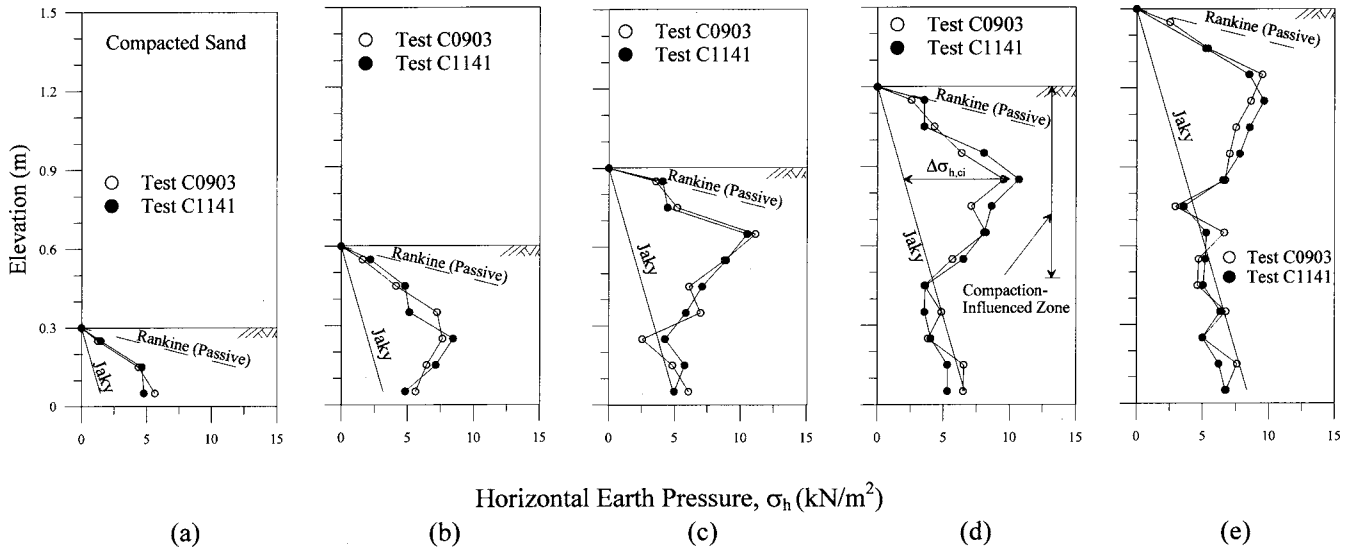

Fig. 5. Distribution of horizontal earth pressure after compaction

zontal earth pressure in the at-rest condition. It may be concluded that for a loose backfill, the vertical stress in the backfill can be properly estimated with the equation $\sigma_v = \gamma z$. The horizontal earth pressure against the nonyielding wall can be estimated with the appropriate application of Jaky's equation.

Stresses in Compacted Sand

To obtain the expected dense condition, the loose backfill was placed and compacted in five lifts. Fig. 4(a) shows the vertical pressure profile after vibratory compaction. In the figure, the measured vertical stresses increased with increasing depth. The vertical overburden pressure can also be properly estimated with the equation $\sigma_v = \gamma z$. As compared with σ_v for loose sand, the overburden pressure measured in dense sand was slightly greater because the compacted backfill had a slightly higher unit weight. It is clear in Fig. 4(a) that compaction did not result in any residual stress in the vertical direction. It may be concluded the effects of vibratory compaction on the vertical pressure in the backfill were insignificant.

The distribution of horizontal earth pressure against the nonyielding wall after the compaction of soil Lift 1 to Lift 5 is shown in Figs. 5(a–e). Each compacted lift was 0.3 m thick after compaction. The variation of lateral earth pressure was monitored by the soil pressure transducers mounted on the wall. Before compaction, Fig. 4(b) shows that the earth pressure at rest can be properly estimated with Jaky's equation. However, after vibratory compaction, it is clear in Figs. 5(a–e) that an extra horizontal normal stress $\Delta\sigma_{h,ci}$ was induced by compaction. Based on the test results of a special 15-day-long experiment (Test C0809), it was found that the extra horizontal stress induced by compaction $\Delta\sigma_{h,ci}$ remained unchanged in the passive zone for at least 2 weeks. Experimental data (Tests C1172, C1162, C0903, and C0106) showed that both the depth of the compaction-induced zone and the extra horizontal stress induced by compaction $\Delta\sigma_{h,ci}$ increases with increasing number of lifts compacted for the same soil mass or the amount of compaction energy input. The lateral stress distribution measured near the top of the backfill was almost identical to the passive earth pressure estimated with Rankine theory. From Figs. 5(a–e), it is interesting to note that the compaction-influenced zone rose with the rising compaction surface. It was also interesting to note in Figs. 5(c–e) that, below the compaction-influenced zone, the measured horizontal stresses converged to the earth pressure at rest based on Jaky's equation. However, it should be emphasized that in Fig. 4(a) the influence of vibratory compaction on vertical stress σ_v in the soil mass is insignificant. In Fig. 5, data points obtained from Tests C0903 and C1141 indicated that the experimental results were quite reproducible.

The stress paths of σ_v versus σ_h for soil elements adjacent to the surface of the nonyielding wall are displayed in Fig. 6. Test data shown in Fig. 6(a) were measured by SPT 2 and SPT 102. In the figure, the path F1 represents the stress variation due to the "filling" of the loose Lift 1. It is clear that the stress path F1 is in good agreement with Jaky's prediction. The filling of sand Lifts 1–5 (stress paths F1–F5) caused an obvious increase in vertical pressure.

Stress path C1 represents the stress variation due to the "compaction" on the surface of soil Lift 1. During the compaction of soil Lift 1 (stress path C1), the lateral earth pressure σ_h measured by SPT2 on the nonyielding wall increased significantly, but the vertical normal stress in soil mass was not affected by compaction. The compaction on Lift 2 (stress path C2) caused the σ_h to increase further. However, the compaction on the surface of Lift 3 resulted in a lateral pressure reduction at SPT2 as indicated by the stress path C3. The compaction on the surface of Lifts 3 and 4 gradually brought the soil element located in front of SPT2 back to an at-rest stress condition. The horizontal earth pressure change was mainly caused by the compaction process, not soil filling. Similar trends can also be observed in Figs. 6(b and c).

Based on the test data shown in Figs. 4–6, it would be reasonable to ask the following four questions: (1) What is the mechanism in the soil mass due to vibratory compaction on the surface of a cohesionless soil? (2) Why would vibratory compaction result in an increase of stress only in the horizontal direction, but not in the vertical direction? If there existed locked-in stresses among soil particles (Sherif et al. 1984), why were the stresses always locked horizontally? (3) Why does the compaction-influenced zone rise with the rising compaction surface? (4) With

J. Geotech. Geoenviron. Eng. 2008.134:437-444.

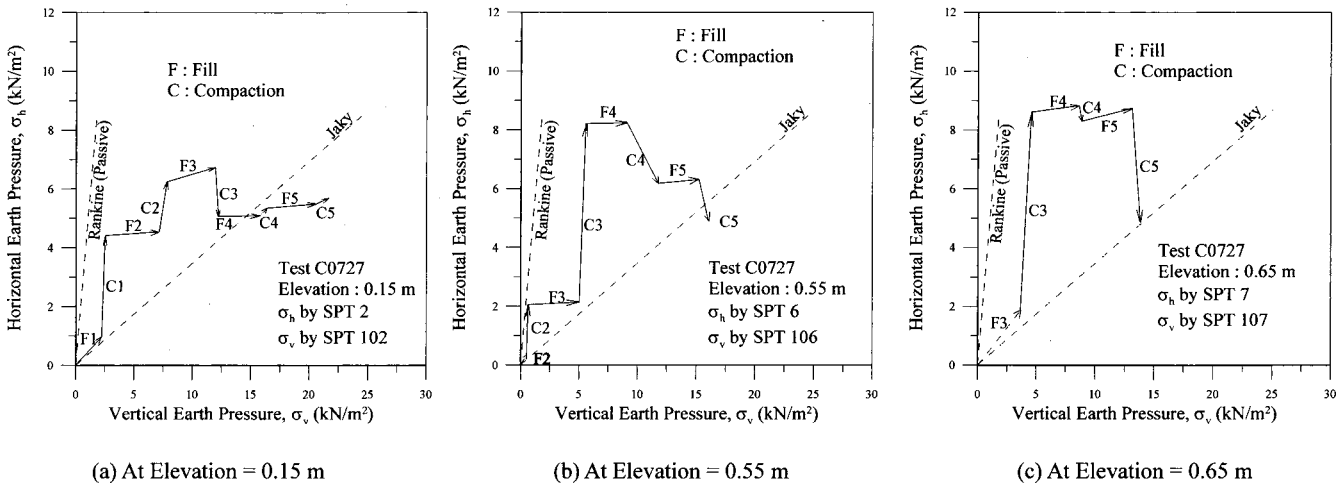

Fig. 6. Stress paths for soil element under filling and compaction of backfill

the rise of the compaction surface, why does the horizontal stress measured below the compaction-influenced zone gradually converge to the Jaky state of stress?

Soil Behavior in Compacted Backfill

In this study, the mechanism of vibratory soil compaction is of central interest. Based on the experimental data, the bearing capacity failure of a surface footing is used to interpret the mechanism of soil behavior due to vibratory compaction.

The proposed mechanism of vibratory compaction on a cohesionless soil can be explained with the help of Fig. 7(a). If the cyclic compacting stress σ_{cyc} applied on the surface of fill exceeded the ultimate bearing capacity q_{ult} of the foundation soil, the loaded surface *ab* would settle and a shear failure zone would develop in the uppermost layer of fill. Terzaghi (1943) reported that as the loaded soil fails, the composite failure surface would develop along either acd_1e_1 or *bcde* shown in Fig. 7(a). Because of the friction and adhesion between the soil and the base of the footing, Zone I remains in an elastic state. Zone II is known as the zone of radial shear, and Zone III is identical to the passive Rankine zone. In Fig. 7(a), if the surface loading at *ab* exceeded q_{ult}, the soil element A would be in the passive Rankine zone. For the soil element under lateral compression, the vertical overburden pressure σ_v remains unchanged; however the horizontal stress σ_h would increase up to the Rankine passive pressure. The moving and compacting of the tamper all over the soil surface would result in a passive soil layer near the top of the compacted fill.

The ultimate bearing capacity q_{ult} of a compacted sandy fill was calculated and compared with the downward cyclic stress applied by the vibratory compactor in this paragraph. Vesic (1973) reported that the bearing capacity failure in soil could be divided into three categories including general shear failure, local shear failure, and punching shear failure as shown in Fig. 7(b). For this study, Fig. 3 showed that the relative density of soil near

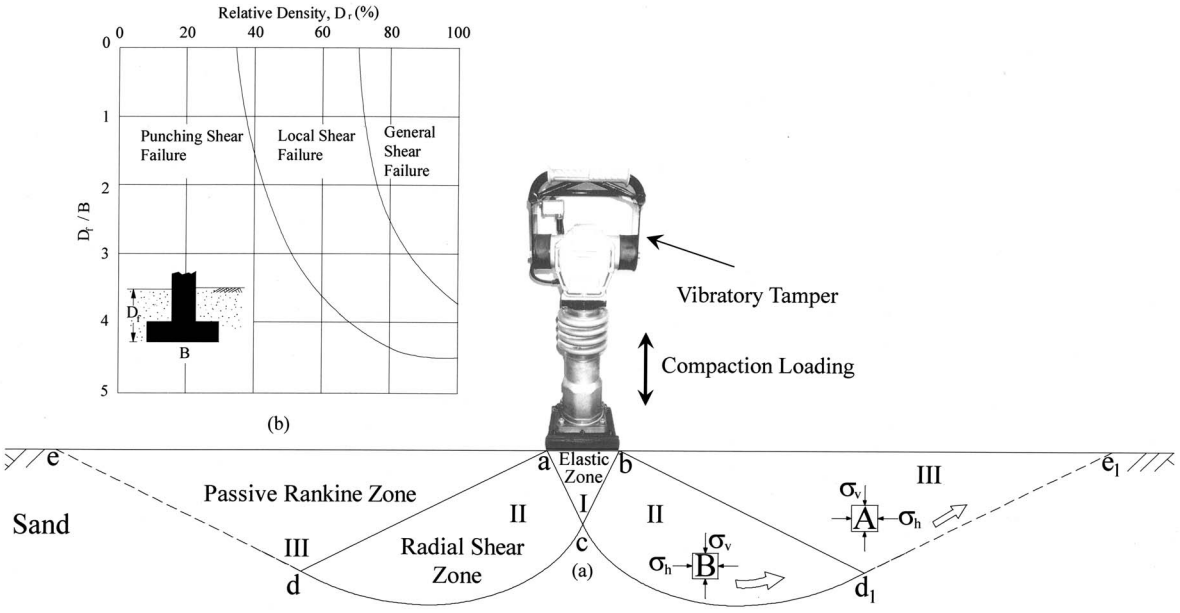

Fig. 7. (a) Bearing capacity failure in soil due to compaction; (b) modes of bearing capacity failure in sand (adapted from Vesic 1973)

J. Geotech. Geoenviron. Eng. 2008.134:437-444.

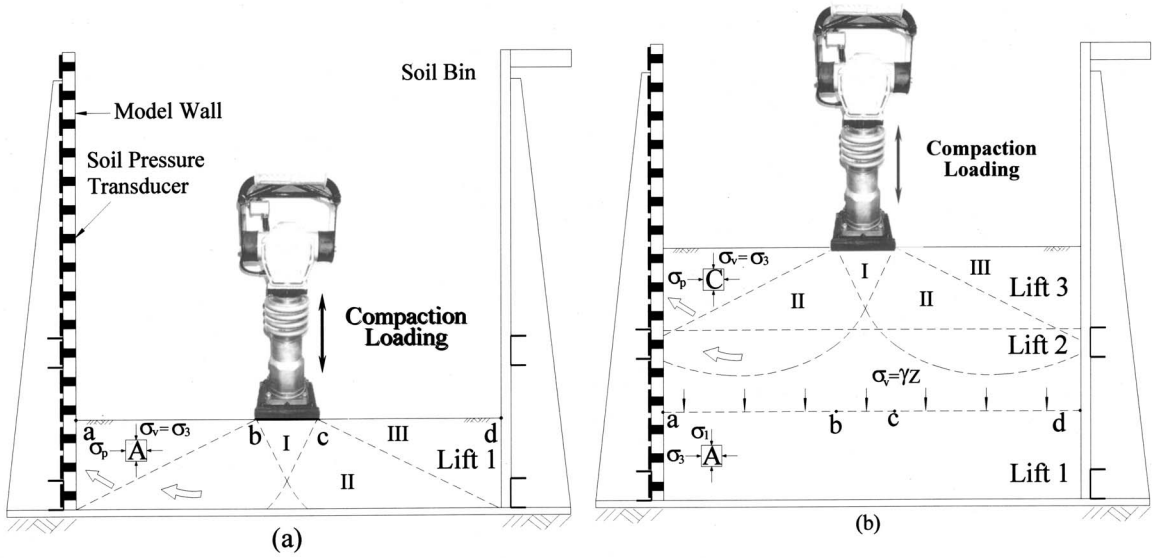

Fig. 8. (a) Vibratory compaction on surface of Lift 1; (b) vibratory compaction on surface of Lift 3

the top of the backfill varied from 55 to 75%. Based on Fig. 7(b), it was assumed that local shear failure would occur due to the application of an unbearable surface loading. On average the relative density of soil measured within 0.5 m below the soil surface was about 68.6%. Based on the results of direct shear tests on air-dry Ottawa sand, the corresponding internal friction angle $\phi = 39.7°$, and the unit weight of the soil was 16.4 kN/m^3. For the foundation soil under a dynamic loading, Vesic (1973) suggested that the static bearing capacity analysis also might be applicable with a reduction of ϕ angle up to 2°. For shallow foundations that exhibited local shear failure mode in soils, Terzaghi (1943) suggested that the bearing capacity factors could be calculated by replacing ϕ with $\phi' = \tan^{-1}(2/3 \tan \phi)$. For this study, the internal friction angle used to estimate the ultimate bearing capacity was $\phi' = 27.2°$. Based on Terzaghi theory, the ultimate bearing capacity for the 0.225 m × 0.225 m square footing on the sandy fill would be $q_{ult} = 17.8$ kN/m^2. Nevertheless, based on the theory proposed by Meyerhof (1963), the calculated $q_{ult} = 23.0$ kN/m^2. It was apparent that the amplitude of downward cyclic dynamic stress $\sigma_{cyc} = 34.9$ kN/m^2 applied by the vibratory compactor exceeded the ultimate bearing capacity q_{ult} of the foundation soil. As a result, the mechanism in the soil mass due to a vibratory compaction of this magnitude on the surface of a cohesionless soil can be described with the bearing capacity failure model proposed by Terzaghi (1943). This answers question (1) raised in the previous section. In the passive Rankine zone, after vibratory compaction, the vertical stress is not affected by the application of σ_{cyc} while the horizontal stress in the zone increased to the passive earth pressure. This answers question (2) raised in the previous section

For the compaction of cohesionless soil in the field, Duncan et al. (1991) summarized the dynamic total forces due to five different types of soil compactor. For vibratory-plate soil compactors, assuming the contact pressure between the plate and soil was uniform, the total (static + dynamic) cyclic pressure applied to the soil surface varied from 32.4 to 101.0 kN/m^2. For rammer-plate soil compactors, the total pressure applied varies from 72.2 to 175.6 kN/m^2. It is obvious that the total loading due to the heavy compaction equipment in the field could easily exceed the bearing capacity of the sandy fill. In the field, it is highly possible that the bearing capacity failure shown in Fig. 7(a) could occur due to the heavy compacting loading acting on the soil surface.

The rise of the compaction-influenced zone with the rising compaction surface phenomenon could be explained with the help of Fig. 8. In Fig. 8(a), compaction was applied on the surface of soil Lift 1. Since $\sigma_{cyc} > q_{ult}$, the soil element A in the passive zone had been compressed laterally, causing high lateral stresses in Lift 1. In Fig. 8(b), after compacting Lifts 1 and 2, the tamper acted on top soil of Lift 3. The passive failure zone rose to a higher elevation, and the soil element C in the passive zone would be compressed laterally. This answers question (3) raised in the previous section why the compaction-influenced zone shown in Fig. 5 rose with rising compaction surface.

It should be noted in Fig. 8(a) that, during compaction of soil Lift 1, there was a strong cyclic stress acting on surface *bc*. Surface *cd* was stress free and was allowed to heave. In Fig. 8(b), tamping acted on top of soil Lift 3, and the passive zone rose with the compaction. Since the strong vertical stress that previously acted at surface *bc* had been removed, and surface *cd* was no longer stress free, the stress condition at the boundary *abcd* changed completely. In this study, the Ottawa sand in the soil box was deposited by the air pluviation method. Fig. 4(a) shows for both the loose and compacted backfills, that the vertical overburden pressure can also be properly estimated with the equation $\sigma_v = \gamma z$. The vertical stress in the soil mass simulates that in a naturally deposited soil mass. Because of the existence of the relatively rigid model wall, the soil element next to the steel wall can be neither stretched nor compressed in the horizontal direction. As a result, the horizontal stress measured below the passive Rankine zone would converge to the earth pressure at rest as indicated in Fig. 5(e). This answers question (4) raised in the previous section why horizontal stresses measured below the compaction-influenced zone converged to the Jaky at-rest state of stress.

In Fig. 9, the experimental test results are compared with the design recommendations proposed by Broms (1971), NAVFAC DM-7.2 (US Navy 1982), Duncan and Seed (1986), Peck and Mesri (1987), and Duncan et al. (1991). Parameter values used in the pressure calculation such as the unit weight γ, relative density D_r, internal friction angle ϕ, wall friction angle δ, and cyclic

J. Geotech. Geoenviron. Eng. 2008.134:437-444.

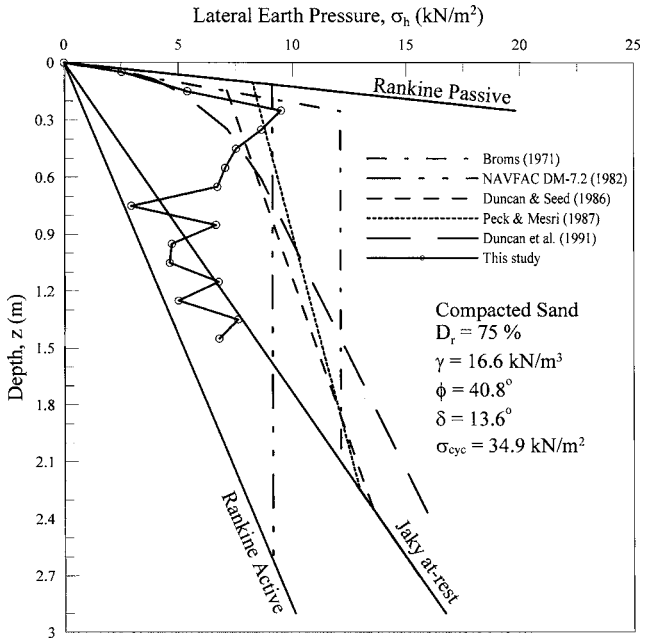

Fig. 9. Horizontal earth pressure estimated with various methods after compaction

compaction stress σ_{cyc} are shown in Fig. 9. The horizontal pressure distribution suggested by the *Navy Design Manual DM-7.2* was based on the analytical method proposed by Ingold (1979). The pressure distribution determined with the method proposed by Duncan et al. (1991) was obtained from the design chart for vibratory plates with a cyclic compaction stress $q=34.9$ kN/m^2 (5 psi).

It may be observed in Fig. 9 that, at a depth less than 0.3 m, the test data are in fairly good agreement with the proposed design methods. The horizontal stresses in the uppermost compacted lift are equal to or slightly less than the passive Rankine pressure. However, at a greater depth, the test data obtained in this study are apparently lower than the calculated horizontal stresses. It should be mentioned that most of the design recommendations are based on or have been compared with full scale tests performed in the field. For this study, the size of the vibratory plate is small (0.225 m $\times$ 0.225 m). It can be deduced with the help of Fig. 7 that the depth of the passive Ranking zone induced by a small compacting plate would be shallower than that induced by a full-size compactor in the field. It should be mentioned that this paper is intended to report on the preliminary experimental data obtained from a 1.5 m $\times$ 1.5 m $\times$ 1.5 m laboratory model. It is obvious that the application of the test findings of this study are limited to estimating the horizontal stresses acting on a nonyielding wall induced by a small size vibratory hand tamper.

Conclusions

Based on the experimental data obtained during this investigation, the following conclusions can be drawn.

1. For a loose backfill, the vertical stress in the backfill can be properly estimated with the traditional equation $\sigma_v=\gamma z$. The horizontal earth pressure against the nonyielding wall can be estimated with the appropriate application of Jaky's equation;
2. For a compacted dense backfill, the vertical overburden pressure can also be properly estimated with the equation $\sigma_v=\gamma z$. The effects of vibratory compaction on the vertical pressure in the backfill were insignificant;
3. After compaction, the lateral earth pressure measured near the top of the wall was almost identical to the passive earth pressure estimated by Rankine theory. If the cyclic compacting stress applied on the surface of the backfill exceeded the ultimate bearing capacity of the foundation soil, a shear failure zone would develop in the uppermost layer of soil. For a soil element under lateral compression, the vertical overburden pressure would remain unchanged, and the horizontal stress would increase to the Rankine passive pressure;
4. The compaction-influenced zone rose with the rising compaction surface. After compacting the lower lifts of soil, the tamping operation was moved to the surface of the top soil lift. The passive zone rose and the soil element in the passive zone was compressed laterally; and
5. Below the compaction-influenced zone, the measured horizontal stresses converged to the earth pressure at-rest condition based on Jaky's equation. As the tamping operation moved to the top soil lift, the strong vertical stress that previously acted at the surface of the lower lift was removed, and the vertical stress acting on the surface of the lower lift became a uniform overburden pressure distribution $\sigma_v=\gamma z$. This is the reason why the horizontal earth pressure measured below the compaction-influenced zone converged to the Jaky state of stress.

Acknowledgments

The writers wish to acknowledge the National Science Council of the Republic of China government Grant No. (NSC 89-2211-E-009-092) for the financial assistance that made this investigation possible. Special thanks are extended to Ying-Chieh Ho, Shin-Yu Chang, Chien-Ting Chen, Si-Kai Tzeng, Shi-Han Tzeng, and Yu-Lun Chien for their assistance.

References

Broms, B. (1971). "Lateral earth pressures due to compaction of cohesionless soils." *Proc., 4th Int. Conf. Soil Mechanics*, Budapest, Hungary, 373–384.

Chen, T. J. (2003). "Earth pressure due to vibratory compaction." Ph.D. dissertation, National Chiao Tung Univ., Hsinchu, Taiwan.

Chen, T. J., and Fang, Y. S. (2002). "A new facility for measurement of earth pressure at-rest." *Geotech. Eng.*, 33(3), 153–159.

D'Appolonia, D. J., Whitman, R. V., and D'Appolonia, E. (1969). "Sand compaction with vibratory rollers." *J. Soil Mech. and Found. Div.*, 95(1), 263–284.

Duncan, J. M., and Seed, R. B. (1986). "Compaction-induced earth pressures under K_o-conditions." *J. Geotech. Engrg.*, 112(1), 1–22.

Duncan, J. M., Williams, G. W., Sehn, A. L., and Seed, R. B. (1991). "Estimation earth pressures due to compaction." *J. Geotech. Engrg.*, 117(12), 1833–1847.

Fang, Y. S., Chen, T. J., Holtz, R. D., and Lee, W. F. (2004). "Reduction of boundary friction in model tests." *Geotech. Test. J.*, 27(1), 1–10.

Ingold, T. S. (1979). "The effects of compaction on retaining walls." *Geotechnique*, 29(3), 265–283.

Jaky, J. (1944). "A nyugalmi nyomas tenyezoje (The coefficient of earth pressure at rest)." *Magyar Mernok es Epitesz-Egylet Kozlonye*, Hungary, 355–358 (in Hungarian).

Meyerhof, G. G. (1963). "Some recent research on the bearing capacity of foundations." *Can. Geotech. J.*, 1(1), 16–26.

J. Geotech. Geoenviron. Eng. 2008.134:437-444.

Peck, R. B., and Mesri, G. (1987). "Discussion of 'Compaction-induced earth pressure under K_o-condition.'" *J. Geotech. Engrg.*, 113(11), 1406–1408.

Sherif, M. A., Fang, Y. S., and Sherif, R. I. (1984). "K_a and K_o behind rotating and nonyielding walls." *J. Geotech. Engrg.*, 110(1), 41–56.

Terzaghi, K. (1943). *Theoretical soil mechanics*, Wiley, New York.

US Navy. (1982). *Foundations and earth structures, NAVFAC design manual DM-7.2*, Washington, D.C.

Vesic, A. S. (1973). "Analysis of ultimate loads of shallow foundations." *J. Soil Mech. and Found. Div.*, 99(1), 45–73.

J. Geotech. Geoenviron. Eng. 2008.134:437-444.